



Distinct cellular microenvironment with cytotypic effects regulates orderly regeneration of vascular tissues

Jian Wang^{a,b,1}, Xun Yang^{c,d,1}, Miaomiao Xu^{a,e}, Hui Liu^{a,e}, Lijun Liu^{c,d}, Zhikai Tan^{a,b,e,*}

^a College of Biology, Hunan University, Changsha, 410082, China

^b Institute of Shenzhen, Hunan University Shenzhen, 518000, China

^c Department of Traumatic Orthopedics, Shenzhen Second People's Hospital (The First Affiliated Hospital, Shenzhen University), Shenzhen, 518028, China

^d Guangdong Key Laboratory for Biomedical Measurements and Ultrasound Imaging, National-Regional Key Technology Engineering Laboratory for Medical Ultrasound, School of Biomedical Engineering, Shenzhen University Medical School, Shenzhen, 518060, China

^e Greater Bay Area Institute for Innovation, Hunan University, Guangzhou, 511300, China

ARTICLE INFO

Keywords:

Cell type specificity
Extracellular matrices
Tissue regeneration
Vascular graft

ABSTRACT

Regeneration of the architecturally complex blood vascular system requires precise temporal and spatial control of cell behaviours. Additional components must be integrated into the structure to achieve clinical success for *in situ* tissue engineering. Consequently, this study proposed a universal method for including any substrate type in vascular cell extracellular matrices (VCEM) via regulating selective adhesion to promote vascular tissue regeneration. The results uncovered that the VCEM worked as cell adhesion substrates, exhibited cell type specificity, and functioned as an address signal for recognition by vascular cells, which resulted in matching with the determined cells. The qPCR and immunofluorescence results revealed that a cell type-specific VCEM could be designed to promote or inhibit cell adhesion, consistent with the expression patterns of eyes absent 3 (Eya3). In addition, a 3D vascular graft combined with VCEM which could recapitulate the vascular cell-like microenvironment was fabricated. The vascular graft revealed a prospective role for cellular microenvironment in the establishment of vascular cell distribution and tissue architecture, and potentiated the orderly regeneration and functional recovery of vascular tissues *in vivo*. The findings demonstrate that differential adhesion between cell types due to the cellular microenvironment is sufficient to drive the complex assembly of engineered blood vessel functional units, and underlies hierarchical organization during vascular regeneration.

1. Introduction

Limited options are currently available for vascular tissue repair and reconstruction [1–3]. Surgical approaches to treat vascular tissue lesions and defects can utilize autologous tissue harvested from the patient to provide a living implant for reconstruction [4,5]. Although natural blood vessels replicate many attributes of living tissue, patients experience significant variability in their individual defect sizes and anatomical locations, typically leading to comorbidities related to mismatches [6,7]. One considerable challenge of currently available implants is their lack of growth potential, which can ultimately result in thromboembolic complications [8,9]. The unpredictability of these procedures can result in costly secondary surgeries that are limited by the physiological conditions of each patient [10]. There is a significant need for a biomaterial

solution that provides the benefits of autologous vascular tissue and has the ease of use and delivery of synthetic implants.

Biomaterials derived from the extracellular matrix (ECM) within cellular microenvironment can be used for tissue regeneration [11–15]. These ECM-based biomaterials, known as matrices or scaffolds, comprise a network of structural proteins and proteoglycans that provide both mechanical support and biological cues for cell migration and tissue development [16–18]. Biological cues from the ECM, including growth factors and ECM-associated vesicles, promote cell migration and tissue development within the implanted acellular scaffolds, gradually leading to the formation of new viable tissue that is potentially permanent [19–21]. Importantly, vessel assembly and maturation are affected by the dynamic nature of the ECM [22–24]. It was reported that both mouse fibroblast-derived and preosteoblast-derived matrices could

* Corresponding author. College of Biology, Hunan University, Changsha, 410082, China.

E-mail address: tanzk@hnu.edu.cn (Z. Tan).

¹ Jian Wang and Xun Yang have contributed equally to this work.

support the vascular morphogenesis of human umbilical vein endothelial cells (HUVECs), but a chondrocyte-derived matrix performed poorly in forming capillary-like structures [25]. Thus, vascular cells might retain their characteristics and essential role in angiogenesis due to their proximity to cell type-specific microenvironmental signals. However, the effects of vascular cell extracellular matrices (VCEM) in the microenvironment on vascular tissue architecture remain unknown due to the difficulty in isolating and obtaining VCEM from native vascular tissue.

The regeneration of blood vessels is a fundamental issue in the engineering design of damaged tissues (including skin, nerves, muscles, and bones), providing nutrients and oxygen to cells buried deep inside the tissue while removing waste away from the cells. Following angiogenesis activation, vascular cells are programmed to form a three-layer structure [26]. The hierarchical vascular tissue is organized spatially to provide adequate nutrients to the cells of all organs and supporting structures [27]. Spontaneous programmed adhesion to vascular cells influences essential cellular processes required for homing and engraftment; this is a crucial process that allows biomaterials to be transplanted in clinical settings [28–33]. The evolutionarily conserved Notch signalling pathway plays critical roles in controlling multiple aspects of vascular development and function, ranging from proliferation, motility, and lumen formation to vessel stability and cell fate determination [34–36]. Understanding how microenvironment and Notch signalling coordinate to establish spatial patterning units is essential to produce functional vascular tissue.

For this study, a tissue engineering vascular graft with distinct microenvironment was created to investigate its cytotypic regulation of cellular behaviours. Cell type-specific VCEM induced cell-selective adhesion, which positively correlated with the levels of eyes absent 3 (Eya3), a transcriptional regulator. The results suggest that Eya3 is a key cell fate determinant that is positively regulated by Notch. Moreover, it is demonstrated that cytotypic effects resulted in host vascular cell redistribution over the 3D microenvironment *in vivo* and controlled cell behavior for blood vessel regeneration to establish a functional native match for cell type and spatial patterning.

2. Materials and methods

2.1. Materials

Poly (ϵ -caprolactone, PCL; Mw = 70,000–90,000 Da) pellets and γ -secretase inhibitor (DAPT, N-[N-(3,5-difluorophenacetyl)-L-alanyl]-S-phenylglycine-butylester, C₂₃H₂₆-F₂N₂O₄) were purchased from Sigma-Aldrich (Saint Louis, MO, USA). Haematoxylin-eosin (HE) and Masson's Trichrome (MT) staining kits were purchased from Solarbio (Beijing, China). Analytical reagents, including N,N-dimethyl-formamide, acetone, and ethanol, were all bought from Sinopharm (Beijing, China). Human umbilical vein endothelial cells (HUVECs) and human vascular smooth muscle cells (HVSMECs) were obtained from Cell Bank, Shanghai Institutes for Biological Sciences, and Chinese Academy of Sciences. An Eya3 antibody (G-9) was obtained from Santa Cruz Biotechnology (California, USA). An anti-vinculin antibody (EPR8185) was obtained from Abcam (Cambridge, UK). The Notch1 polyclonal antibody was obtained from ProteinTech Group (Chicago, IL, USA), and the CD31 monoclonal and smooth muscle actin polyclonal antibodies were bought from Affinity Biosciences (Changzhou, China).

2.2. Generation of engineered vascular microenvironment *in vitro*

2.2.1. Preparation of oriented scaffolds

Scaffolds were fabricated using a customized E-jet 3D bio-printing system as previously described [37,38]. In brief, PCL pellets were dissolved in DMF at 7% w/v, and the solution was then used for 3D printing. Aligned PCL fibres were printed precisely in a pre-designed pattern using a 27G nozzle at a volumetric flow rate of 200 $\mu\text{L h}^{-1}$, and the distance to the substrate was approximately 1 mm. A 27 kV voltage

was applied to ensure the completion of the work. The fabricated oriented scaffolds were then disinfected and stored at 4 °C until use.

2.2.2. Preparation of bacterial cellulose membrane

The bacterial cellulose (BC) membrane was acquired by culturing *Bacillus xylinus* (ATCC 23767) in NBRC#350 medium, including 5 g glucose, 1 g MgSO₄·7H₂O, 5 g mannitol, 5 g polypeptone, and 5 g yeast extract in 1 L of deionized water. The medium was sterilized for 20 min at 121 °C, and then 5 mL ethanol was added before inoculating bacteria (10%, v/v). After two weeks, the BC membrane was harvested and rinsed with deionized water, then boiled in 1% NaOH until the solution was clear. Finally, the membrane was rinsed with deionized water until pH 7.0. The collected samples were sterilized and stored at 4 °C for future use.

2.2.3. *In vitro* 3D microenvironment with VCEM

HUVECs were seeded on aligned PCL scaffolds to construct engineered endothelial cell extracellular microenvironment. After 48 h of incubation, the samples were rinsed with phosphate-buffered saline (PBS) and inactivated by repeated freezing and thawing (F/T) to obtain 3D HUVEC ECM microenvironment (3D EHUVEC) where ECM components were maintained, but cellular components were eliminated. In brief, the samples were subjected to three F/T cycles using a –80 °C freezer and a 37 °C water bath. For the first cycle, the samples were stored at –80 °C for 24 h. After the samples returned to room temperature, they were rinsed with PBS 3 times. After freezing for another 24 h, the samples were placed in distilled water for 2 h to induce hypotonic shock and cytolysis of any remaining cells. After the final F/T cycle, the samples were rinsed again with PBS. All procedures were carried out in a biological safety cabinet or a sterile environment. Similarly, HVSMECs were inoculated on the BC membranous scaffolds to construct engineered 3D HVSMEC ECM microenvironment (3D EHVSMC). The methods were the same as those used for the engineered 3D EHUVEC. Scanning electron microscopy (SEM) and histological analyses were used to assess the decellularization process.

2.3. Water contact angle test

The surface water contact angles of the specimens were tested using the sessile drop method in air at room temperature. A video optical contact angle measuring instrument (DSA100, KRÜSS, Germany) was used, and the drop size was set to 10 μL .

2.4. Fabrication of engineered vascular grafts

The constructed vascular grafts had two layers. The outer layer was made using a BC membrane, and the inner layer comprised oriented PCL fibrillar scaffolds. The layers were attached to each other under wet conditions. The composite scaffold was then rolled up using a stainless-steel mandrel (1.2-mm diameter) with the fiber direction perpendicular to the direction of movement; this ultimately formed a two-layered tubular structure. Bioengineered vascular grafts containing 3D EHUVEC and EHVSMC microenvironment were constructed after seeding and removing varied cells as mentioned above.

2.4.1. Scanning electron microscopy

Engineered blood vascular grafts were fixed overnight in 4% paraformaldehyde at 4 °C and dehydrated with graded ethanol solutions (30, 50, 75, and 100% EtOH), followed by critical point drying. The specimens were coated with gold and examined using a scanning electron microscope (QUANTA 200, FEI, USA) at an accelerating voltage of 20 kV, and a JSM-6700F scanning electron microscope (JEOL, Japan) at an accelerating voltage of 5 kV.

2.5. Immunofluorescence staining

Cell specimens were fixed in 4% PFA for 15 min, followed by permeabilization with 0.2% Triton-X for 10 min; the samples were blocked with normal goat serum (ready-to-use, Boster AR0009) for 30 min at room temperature. Primary antibodies were diluted 1:100 in PBS and incubated overnight at 4 °C. After rinsing three times with PBS, the specimens were incubated with secondary antibodies for 2 h in the dark. All cells were counterstained with DAPI. The immunofluorescence images were obtained using an OLYMPUS FV1200 confocal microscope, and quantitative analyses were conducted using ImageJ.

2.6. Quantitative polymerase chain reaction (qPCR)

RNA was isolated with an RNAiso Plus kit (Takara, Japan) and quantified using a NanoDrop2000 Spectrophotometer (ThermoFisher). cDNA synthesis was performed using an inNova Uscrip All in One First-Strand cDNA Synthesis SuperMix kit (Innovagene, China). qPCR analysis was conducted using 2 × inNova Taq SYBR Green qPCR Mix (Innovagene, China) and a CFX96 Touch™ Real-Time PCR Detection System (Bio-Rad, Singapore). The specimens were analysed in triplicate, and fold changes in expression were determined using the comparative $\Delta\Delta C_T$ method. GAPDH was used as an endogenous control, and the primer sequences are detailed in Table S1.

2.7. Animal experiments

An abdominal aorta replacement model was established using Sprague Dawley (SD) rats (aged 10 weeks and weighing 280–320 g) purchased from Hunan SJA Laboratory Animal Co., Ltd. (Changsha, China). The animal experiments were approved by the Animal Experiments Ethical Committee of Hunan University (Permit No. HNU-BIO202101009) and complied with the Guide for the Care and Use of Laboratory Animals. The rats were anaesthetized by intraperitoneal injection of 5% chloral hydrate (7 mL/kg); approximately 10 min was allowed to pass to allow the animals to enter deep anaesthesia before the operation. The rats were fixed on an operating table, and their abdominal hair was removed. Then, the abdominal aorta was exposed by blunt separation, and a vascular clip was used to clamp and cut. Next, a 7-0 suture needle was used to suture the engineered blood vessel grafts end-to-end, with 8–10 stitches at each end.

2.8. Ultrasound imaging

Ultrasound imaging with a Vevo 2100 ultrasound platform (Visual Sonics, Toronto, Canada) was used to monitor the neoartery patency and diameter changes of the vascular grafts *in vivo*. The same neoartery was imaged over time at 4, 12, and 24 weeks after implantation. B-mode and pulsed-wave Doppler mode were used to determine the position and patency of the grafts, respectively. Flow profiles were confirmed using colour Doppler mode, and M-mode images were used to monitor diameter changes of the neoartery after transplantation.

2.9. Mechanical tests

The mechanical strength of the vascular graft or abdominal aorta with a comparable dimension was analysed using a HengWing Tester (HY-0580WN, Shanghai) equipped with a 10 N loaded cell. Specimens were mounted between two stainless steel pins; one of which was attached to an actuator, while the other one was attached to the loaded cell. The longitudinal stress and strain were measured by clamping the samples (2 cm inter-clamp distance) in the testing machine and pulling them at a constant rate of 50 mm/min until failure. Engineering stress was calculated by dividing the tensile force (F) by the total cross-sectional area ($S = \pi * \text{diameter of the graft} * \text{thickness of graft wall}$).

The elongation at break, tensile strength, and elastic modulus of the

specimens were calculated and plotted according to a previously described method. Suture retention strength was determined in accordance with ISO 7198:2016: a 2-cm long graft was clamped at one extremity onto a tensile-testing machine, and the other extremity was bevelled for implantation; a single bite suture was placed 2 mm from the edge (7-0 nylon suture needle with line, Lingqiao, Ningbo Medical Needle Co., Ltd). A constant pulling rate of 120 mm/min was applied until the suture was pulled out. Suture retention measurements were repeated at 120° intervals.

2.10. Histological and immunohistochemical analyses

At 4, 12, and 24 weeks after surgery, the rats were anaesthetized. The abdominal aortas were exposed again via an abdominal incision, and the grafts were removed and rinsed immediately with PBS. For histological analysis, the explanted vascular grafts were fixed with 4% paraformaldehyde (PFA, Beyotime, China) at 4 °C overnight; then, they were paraffin-embedded, sectioned, and stained with HE and MT.

For immunohistochemical analysis, the vascular grafts were embedded vertically into optimal cutting temperature compound (Sakura Finetek, USA), snap-frozen at $-80\text{ }^{\circ}\text{C}$, and cryosectioned at 10- μm -thickness. The slides were prepared for CD31 and α -smooth muscle actin (α -SMA) immunohistochemical staining, and the nuclei were counterstained with DAPI for 5 min. The specimens were visualized using a bond polymer refined detection system (Leica, USA). All histological images were captured with an inverted microscope (Eclipse Ti2, Nikon, Japan) using bright field or polarized light. The HE staining images were then used to quantify the wall thickness of the grafts.

2.11. Statistical analysis

The data are presented as the means \pm SDs. All statistical analyses were carried out using *t*-test or one-way analysis of variance (ANOVA) in Prism 9.0 GraphPad Software (San Diego, CA). $P < 0.05$ was considered statistically significant.

3. Results

3.1. The difference in cell adhesion recapitulates cell-type specificity of the VCEM

Vinculin is a highly conserved intracellular protein with a crucial role in the maintenance and regulation of cell adhesion [39]. To validate the cell type specificity of the VCEM, vinculin was designed to test the adhesion of cells on VCEM (Fig. S1). HUVECs and HVSMECs were cultured with vascular endothelial cell-derived ECMs (EHUVEC) or vascular smooth muscle cell-derived ECMs (EHVSMC) for 48 h; blank TCP was used as a control. The results showed that EHUVEC potently promoted vascular endothelial cell adhesion (via vinculin staining and qPCR), but EHVSMC inhibited this process. Similarly, EHVSMC enhanced vascular smooth muscle cell adhesion, but this was not the case for EHUVEC (Fig. 1a and b). These results demonstrate that specific VCEM played different roles in regulating vascular cell behaviours, confirming that the VCEM had cell-type specificity.

While searching for a regulator of VCEM/cell type interactions, Eya3, a highly conserved transcriptional co-regulator and phosphatase was identified; this molecule is well-characterized for its role as a cell fate determinant [40]. Consistent with the cell type-specific VCEM-related changes in cell adhesion, EHUVEC and EHVSMC respectively affected HUVEC and HVSMEC Eya3 gene expression and protein levels. As expected, VCEM induced Eya3 downregulation in non-source cells (Fig. 1c and d). In fact, Eya3-negative cells may not only lack adhesion with the VCEM but also indicate active rejection, this could be seen from the fact that the level of vinculin was even lower than that of TCP in non-autologous extracellular matrix, both in HUVECs and HVSMECs (Figs. S2a&b). The Eya3 expression patterns and resulting differential

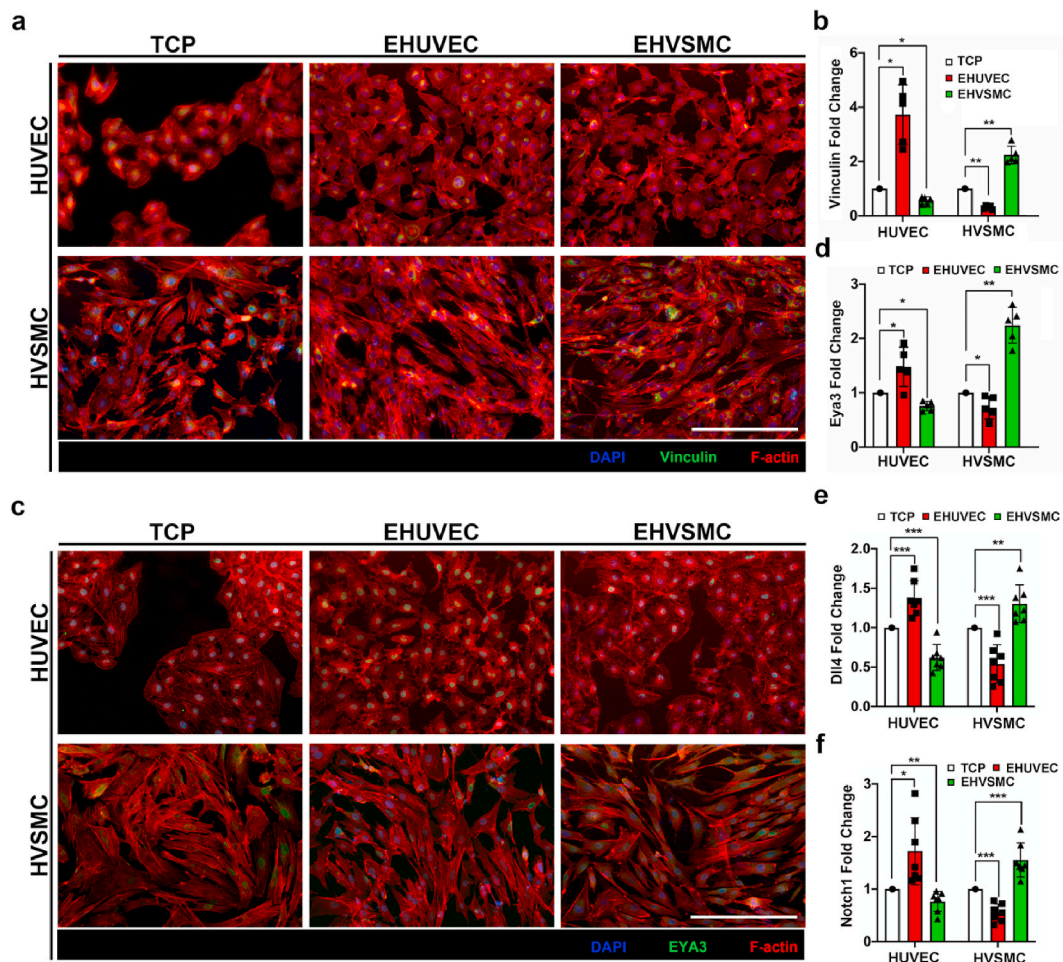


Fig. 1. Cell adhesion was affected by cell-type specific VCEM. Vascular cells were cultured with EHUVEC and EHVSMC for 48 h; blank TCP was used as a control. (a) Representative confocal images showing the adhesion (vinculin, green) and shape (F-actin, red) of HUVECs and HVSMCs after culture with EHUVEC and EHVSMC. (b) Relative mRNA expression of adhesion-related genes in vascular cells. (c) Protein expression of Eya3 in HUVECs and HVSMCs after culture with EHUVEC and EHVSMC. (d) Relative mRNA expression of Eya3 in vascular cells. (e–f) Gene expression of the Notch pathway, including the ligand Dll4 (e) and receptor Notch1 (f). Scale bar = 200 μ m; * p < 0.05; ** p < 0.01; *** p < 0.001. Statistically comparison only with the control group. (For interpretation of the references to color in this figure legend, the reader is referred to the Web version of this article.)

adhesion dictated the vascular cell distribution with the cell type-specific VCEM. Accordingly, linking Eya3 expression with vascular cell fate ensures a robust match between vascular cells adhesion and cell type-specific VCEM.

Notch signaling is among the most important pathways involved in vascular development, which is implicated in Eya expression during tissue self-organization [41]. Therefore, Notch signaling may play a role in the differential adhesion of vascular cells caused by Eya3 expression. Results show that either Dll4 or Notch1, which were downregulated in HVSMCs during culture with EHUVEC, were instead up-regulated in EHVSMC. Similarly, in HUVECs, EHVSMC exposure significantly reduced the expression of genes associated with Notch signals that were increased in EHUVEC (Fig. 1e&f). These results indicated that cell-type specific VCEM may regulate expression patterns of Eya3 through Notch signalling pathway.

3.2. Notch1 blockade reduced Eya3 expression in vascular cells

The Notch1 localization with EYA3 in HUVECs or HVSMCs was assessed. Strong association of Notch1 signals with EYA3 signals (Fig. 2a) was detected, suggesting that Notch1 signals may regulate EYA3. Furthermore, vascular cells were treated with a γ -secretase inhibitor (DAPT, 50 μ M) to inhibit Notch1 signalling activation [42]. Notch1 inhibition was observed in both HUVECs and HVSMCs compared

to TCP as a control group, confirming the effectiveness of the DAPT (Fig. 2a and b). Furthermore, Notch1 protein levels in vascular cells, whether cultured with EHUVEC or EHVSMC, were significantly reduced by DAPT treatment. In short, the immunofluorescence images show that Notch1 blockade inhibited EYA3 signals in HUVECs cultured with EHUVEC, which was similar to the results for HUVECs cultured with EHVSMC without DAPT. Similarly, Notch1 blockade inhibited EYA3 signals in HVSMCs cultured with EHVSMC, which was similar to the results for HVSMCs cultured with EHUVEC without DAPT. Significantly, the vascular cells had impressive EYA3 signals processed by their own matrix (Fig. 1c), which disappeared with the inhibition of notch1. Not surprisingly, the qPCR results also revealed this phenomenon (Fig. 2c). These results indicated that Notch signals may control EYA3 faced with the treatment of cell-type specific VCEM.

To determine the functional role of Notch signalling in regulating Eya3 expression, the effect of Notch1 inhibition on vascular cell adhesion was explored. HUVECs had high vinculin protein expression when cultured with EHUVEC (Figs. S2a&b). However, vinculin protein levels were significantly reduced in DAPT-treated HUVECs compared with controls (Fig. 2d). In HVSMCs, high vinculin protein expression was observed upon culture with EHVSMC, but the protein expression levels were greatly reduced after adding DAPT; these results are similar to those of HVSMCs cultured with EHUVEC (Figs. S3a&b). The qPCR results also demonstrated that DAPT inhibited vinculin gene expression

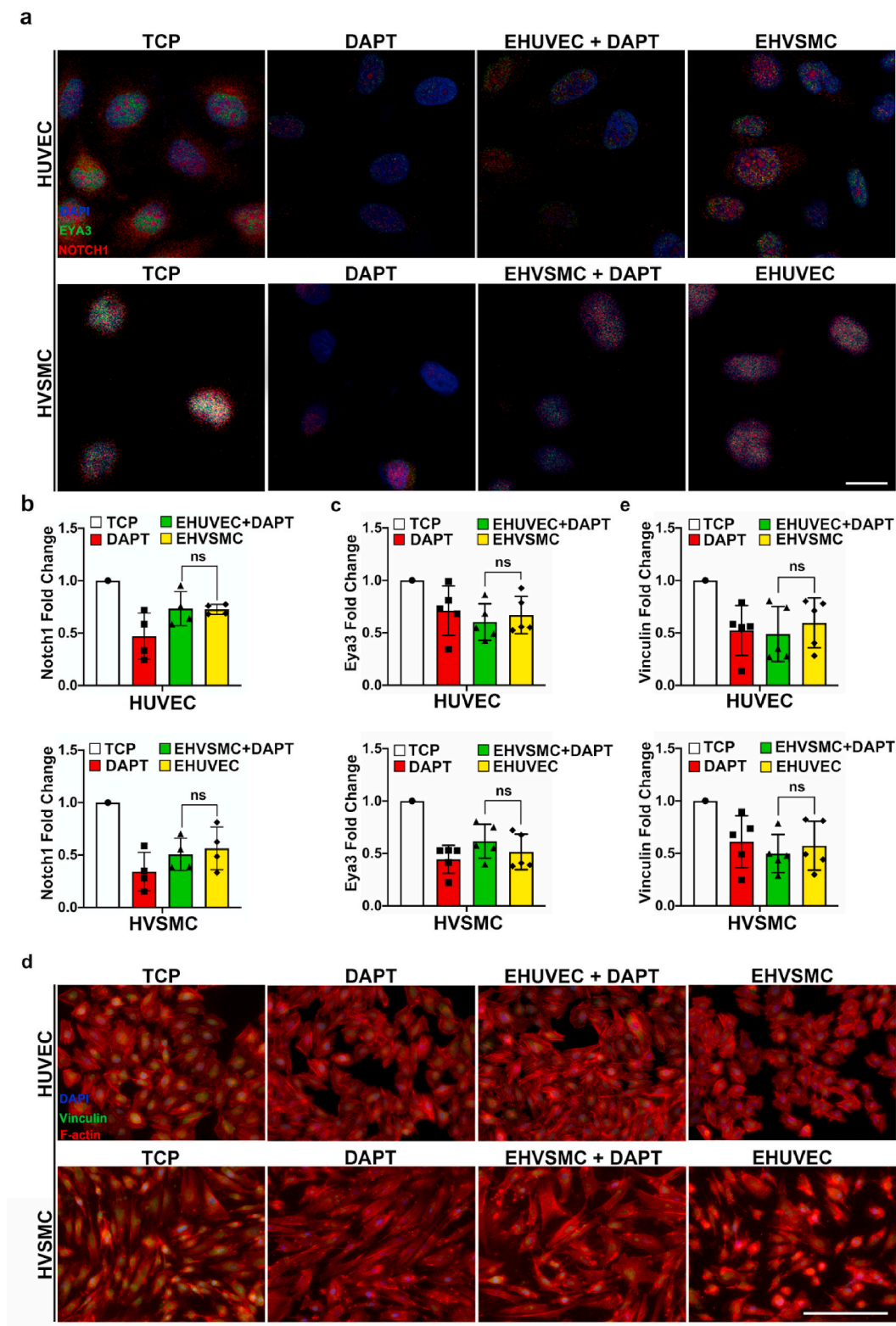


Fig. 2. Eya3 expression patterns and the resulting differential adhesion may require Notch signalling. (a) Images of EYA3 and NOTCH1 co-localization in HUVECs cultured with TCP (untreated), DAPT, EHUVEC with DAPT, and EHVSMC and in HVSMCs cultured with TCP (untreated), DAPT, EHVSMC with DAPT, and EHUVEC. Scale bar = 20 μ m. (b–c) qPCR results showing relative Notch1 (b) and Eya3 (c) expression in HUVECs and HVSMCs from (a). (d) Fluorescence images of vinculin in HUVECs cultured with TCP (untreated), DAPT, EHUVEC with DAPT, and EHVSMC and in HVSMCs cultured with TCP (untreated), DAPT, EHVSMC with DAPT, and EHUVEC. Scale bar = 200 μ m. (e) qPCR results showing relative vinculin expression in HUVECs and HVSMCs from (d). ns indicates not significant.

(Fig. 2e). More importantly, DAPT inhibited the positive effects of the VCEM on its source cells, resulting in the same effects as other cell-derived VCEM and negating the VCEM cell specificity. Taken together, these results indicate that the VCEM coordinated extracellular matrix matching with the vascular cell type through Eya3-mediated selective adhesion, possibly requiring Notch signalling.

3.3. 3D cellular microenvironment with VCEM *in vitro*

For vascular tissue, it is the structural anisotropy and hierarchical organization of the VCEM microenvironment that form its functions [43, 44]. To retain the microtopographical features and microarchitectural structures of the vascular endothelial cell cellular microenvironment *in vitro*, a series of longitudinally aligned PCL microfibres to direct vascular endothelial cell alignment was generated by 3D printing. The frequency distribution of the cell angles showed the preferential orientation for HUVECs at a fibre spacing of 100 μm (Fig. S4). Decellularized VCEM components from HUVECs were used for the surface modification of PCL scaffolds to generate the 3D vascular endothelial cell mimetic culture microenvironment (3D EHUVEC, Fig. 3a and c). Decellularized EHSMC were used to modify BC membranous scaffolds to generate the 3D vascular smooth muscle cell mimetic culture microenvironment (3D EHSMC, Fig. 3b and e). A calcein-AM/PI double-staining assay visually showed abundant cell survival, which confirmed the biocompatibility of the PCL (Fig. 3d) and BC (Fig. 3f) scaffolds. SEM images showed hardly any cells on the scaffolds after decellularization and the preservation of VCEM constituents, indicating the successful surface modification of the PCL (Fig. 3g and h) and BC (Fig. 3i and j) scaffolds with EHUVEC and EHSMC, respectively. To confirm the changes in scaffold surface

properties after VCEM coating, water contact angles were measured after surface modification. The water contact angle of 3D EHUVEC modified PCL scaffolds decreased from $86 \pm 3^\circ$ to $68 \pm 2^\circ$ (Fig. 3k & l), while that of 3D EHSMC modified BC scaffolds changed from $25 \pm 1^\circ$ to $92 \pm 2^\circ$ (Fig. 3m & n).

3.4. 3D microenvironment with VCEM regulated the selective adhesion of vascular cells

Immunofluorescence staining for vinculin showed that 3D EHUVEC significantly increased HUVEC adhesion and effectively guided cell alignment (Fig. 4a), similar to vascular endothelial cells in natural vascular tissues [45]. However, in contrast to HUVECs, HSMC adhesion was inhibited by 3D EHUVEC, and vinculin expression was evidently lower than that of the TCP group. qPCR analysis confirmed that vinculin gene expression in the HUVEC and HSMC groups was the highest and lowest, respectively, when cultured with 3D EHUVEC (Fig. 4b). Vascular cells were also cultured with 3D EHSMC to further show the role of 3D VCEM microenvironment in selectively regulating vascular cell adhesion (Fig. 4c). 3D EHSMC obviously inhibited HUVEC adhesion, as shown by vinculin immunofluorescence staining, but vinculin expression was greatly promoted in HSMCs, also confirmed by qPCR analysis (Fig. 4d). When cultured with 3D EHSMC, vinculin gene expression in the HUVEC and HSMC groups was the lowest and highest, respectively. These results indicate that the 3D VCEM microenvironment significantly promoted the adhesion behaviour of cells from which they are derived (Fig. 4e); furthermore, the selective adhesion of vascular cells was regulated using cell type-specific 3D VCEM. These data clearly supported the fact that the selectively

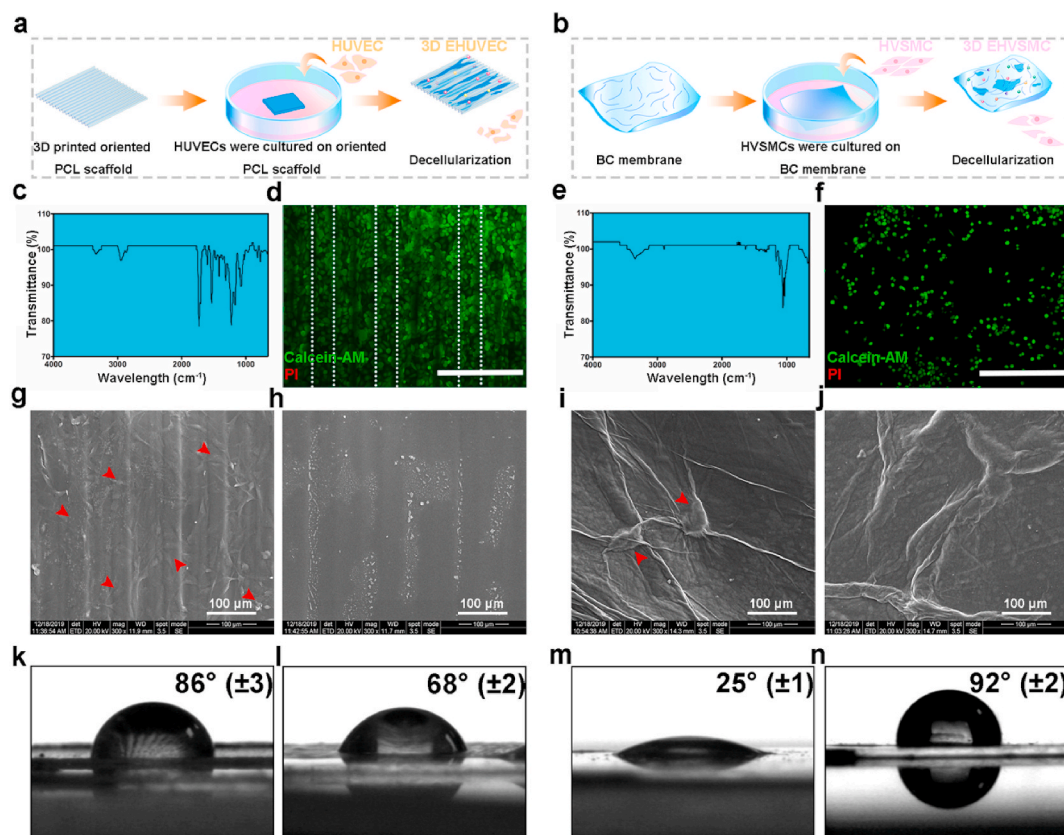


Fig. 3. Reconstruction and characterization of 3D cellular microenvironment with VCEM *in vitro*. (a–b) Schematic of the formation of 3D EHUVEC (a) and EHSMC (b) microenvironment. (c, e) FTIR spectra of PCL (c) and BC (e) scaffolds. (d, f) Calcein-AM/PI fluorescence images (green, living cells; red, dead cells) of HUVECs cultured with PCL scaffolds (d) and HSMCs cultured with BC membranes (f). Scale bar = 400 μm . (g–j) SEM images of 3D EHUVEC before (g) and after (h) decellularization and 3D EHSMC before (i) and after (j) decellularization. (k–n) Static water contact angles of PCL scaffolds (k), 3D EHUVEC (l), BC membranes (m) and 3D EHSMC (n). (For interpretation of the references to color in this figure legend, the reader is referred to the Web version of this article.)

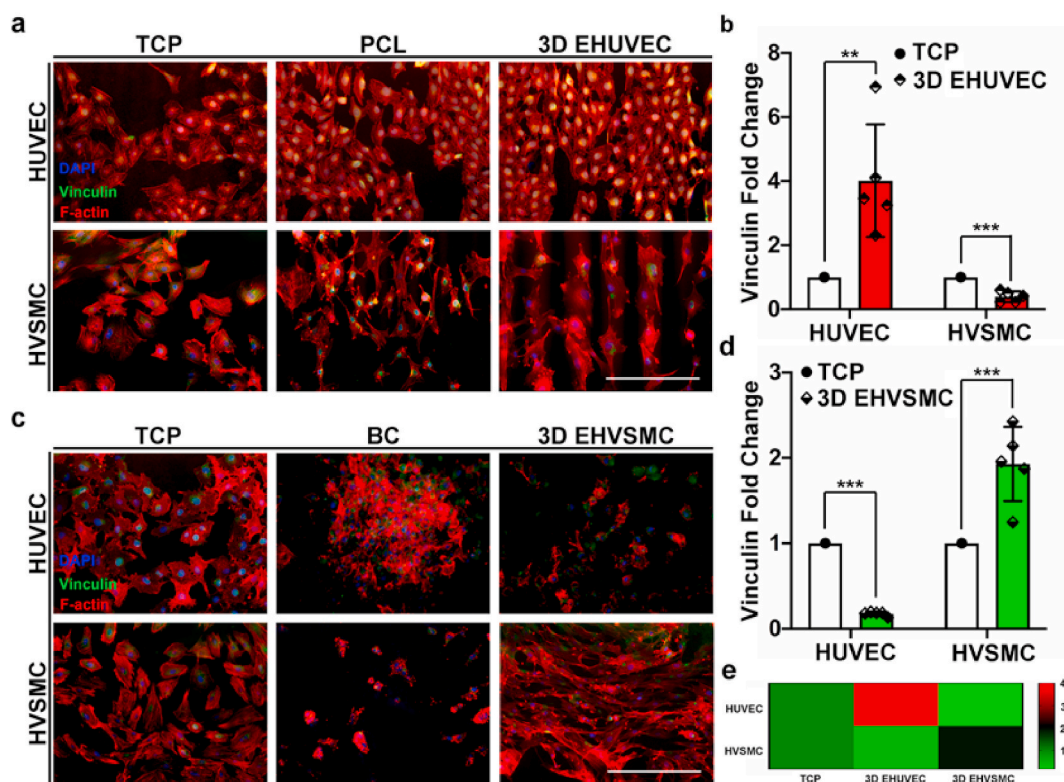


Fig. 4. 3D microenvironment regulated the selective adhesion of vascular cells. (a) HUVEC and HVSMMC adhesion after culture on TCP, PCL scaffolds, and 3D EHUVCE for 48 h as indicated by vinculin immunostaining. (b) Vinculin relative expression levels in HUVECs and HVSMMCs from (a). (c) HUVEC and HVSMMC adhesion after culture on TCP, BC membranes, and 3D EHVSMC for 48 h as indicated by vinculin immunostaining. (d) Vinculin relative expression levels in HUVECs and HVSMMCs from (c). (e) Heatmap showing 3D VCEM of vascular cells can significantly enhance vinculin gene expression in cells from which they are derived. Scale bar = 200 μ m.

adhesion of vascular cell could be regulated by 3D VCEM retained the cell type-specificity of the VCEM (Figs. S2a&b).

3.5. Preparation of bioengineered vascular grafts with distinct cellular microenvironment

Bioengineered vascular grafts (bEVGs) containing 3D EHUVCE and EHVSMC were constructed (Fig. 5a). Since cell type-specific 3D VCEM can regulate selective vascular cell adhesion, we assume that the combination of 3D EHUVCE and 3D EHVSMC could achieve the endogenous induction and localized adhesion of HUVECs and HVSMMCs, respectively, which are critical for vessel regeneration. The vascular grafts provided the needed endogenous stimulus while retaining the microtopographical features and tissue structures. Vascular grafts without acellular VCEM (EVGs) modification were used as a control. The inner diameter of the bioengineered vascular grafts was 1.2 mm (Fig. 5b), and the thickness was $158 \pm 17 \mu$ m. The thickness was not significantly different from that of the control group ($152 \pm 13 \mu$ m). SEM images indicated that the inner and outer layers of the grafts were closely connected, and longitudinally aligned PCL microfibre structures were present in the inner layer. Unlike the controls (Fig. 5c), the experimental grafts had no cells present, but the ECM constituents were preserved in both the inner and outer layers (Fig. 5d). Additionally, no visible nuclei were found in tissue sections stained with H&E (Fig. S5).

3.6. Patency of bEVGs in vivo

To assess the regeneration potential of bEVGs, an abdominal aorta replacement model was established using SD rats (Fig. 6a). EVGs were used as controls. The results showed excellent structural integrity throughout the study for the bEVG group; no aneurysmal dilation was

found, and perfect patency with no thrombosis and limited intimal hyperplasia was achieved. The position and patency of the grafts were monitored *in vivo* using ultrasound imaging (Fig. 6b, c & S6). The bEVG diameters appeared to increase slightly over time after transplantation (Fig. 6d), but the surrounding aorta diameters also increased in the growing juvenile rats (Fig. S6a). The peak systolic velocity of the bEVGs significantly varied during the 24 weeks (Fig. 6e). Furthermore, the EVGs reproducibly expanded with systole and diastole, but the peak systolic velocity significantly decreased over time after grafting, in accordance with the diameter increases (Fig. S6b). No significant differences between bEVGs and native arteries were found, and the bEVGs worked as the rats' own blood vessels over time after transplantation.

3.7. Temporal evaluation of cell infiltration and matrix remodelling

To further explore the potential of bEVGs to promote *in situ* angiogenesis, histological and immunological evaluations of the grafts were performed. Routine HE staining of bEVG cross sections at numerous times after implantation showed that the bEVGs were repopulated with host cells, although the multi-layered structures of the grafts remained visible 4 weeks after transplantation (Fig. 7a). bEVGs became progressively more re-cellularized by host cells over time, with further medial and neointima layer development in the examined specimens. Most notably, the hierarchical organization was significantly optimized in the bEVGs compared with the controls (EVGs, Fig. 7a&b). The dense ECMs of the bEVGs consisted primarily of collagen (Fig. 7c), and CD31 and α -SMA co-staining revealed that thick smooth muscle layers were separated from the blood by a continuous endothelium in the bEVG-guided neo-artery, similar to native arteries (Fig. 7e&g). As expected, the EVGs failed to localize host cells for maturation, and the distribution of host endothelial and smooth muscle cells was unorganized

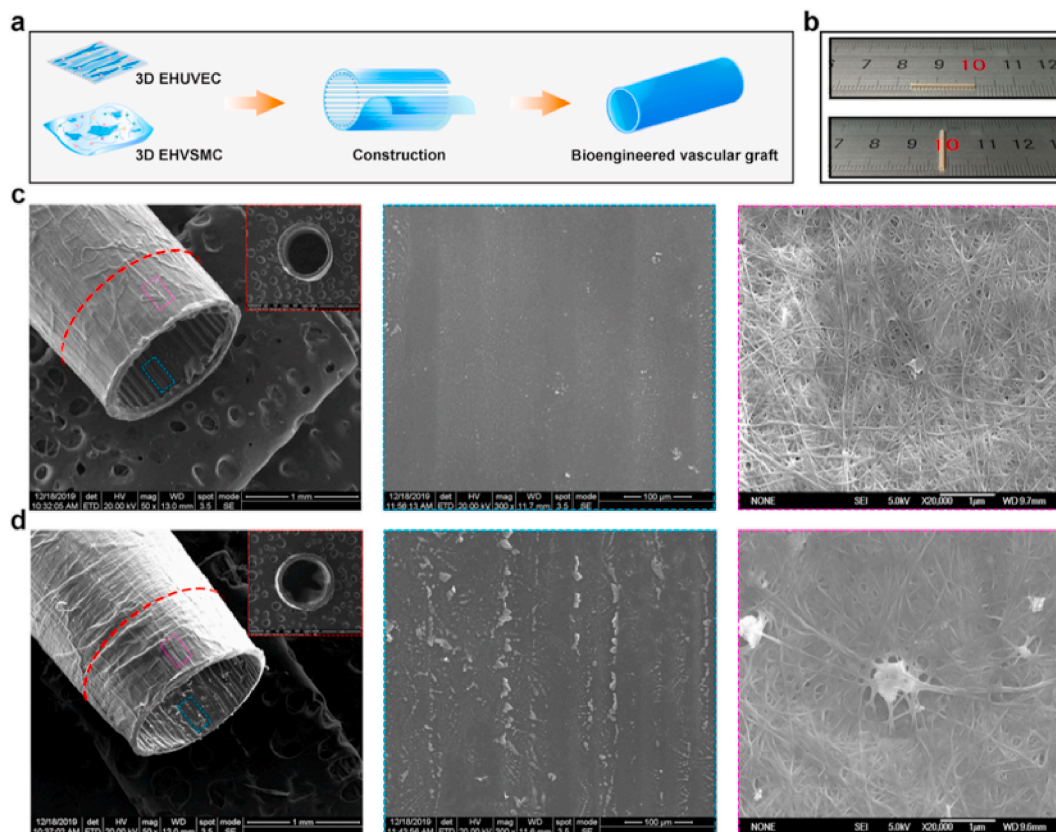


Fig. 5. Ultrastructure of the bioengineered vascular grafts. (a) Pattern diagram of bEVGs. (b) Images of bEVGs (inner diameter = 1.2 mm). (c, d) SEM images of an EVG without VCEM modification (c) and a bEVG composed of 3D VCEM microenvironment (d): sections were taken to examine the matrix architecture; higher magnification of the inner and outer surfaces.

(Fig. 7e&f). From these results, we conclude that a bEVG coated with vascular cell type specific 3D VCEM microenvironment to direct the self-assembly of a mixture of endothelial cells (ECs) and smooth muscle cells (SMCs) *in vivo*.

The mechanical properties of bEVGs were examined using an HY-0580 system to derive stress-strain plots, including elongation at break, tensile strength, suture retention, and elastic modulus (Fig. 8). Not surprisingly, the vascular grafts, including the controls, displayed markedly higher mechanical strength than the native arteries of the rats. Compared with those of EVGs, the mechanical properties of bEVGs with VCEM surface modification did not change significantly. More importantly, the elastic modulus improved in bEVGs at week 24 after transplantation (Fig. 8d), which may benefit from better remodelling *in vivo*. The vascular graft presented above possessed adequate biomechanical properties and the long-term feasibility as substitutes for the native vessel anyway.

4. Discussion

The potential of appropriate re-cellularisation in tissue engineering for vascular regeneration has recently received considerable attention [1]. A key barrier of such applications to clinical settings is adverse host cellular reactions due to inappropriate or insufficient matrix remodeling [4]. During blood vessel development, ECM components within the *in vivo* micro-environment are known to provide diverse dynamic signalling cues that mediate cell migration, proliferation, differentiation, maturation, and survival [32,46]. It was previously found that acellular vessels, generated by seeding human vascular cells into a biodegradable mesh scaffold within a bioreactor system, could be favourably repopulated by host cells. This phenomenon could be explained by the micro-environment remodeling that the cells were exposed to *in vivo*, which

included soluble factors, 3D ECM structures, and dynamic mechanical forces during reprogramming [47]. The ECM is known to be a key component of cellular microenvironment. By providing complex combinations of morphogenetic cues, the ECM is an effective mediator for determining cell fate [48]. Although the importance of the cell micro-environment based on the ECM has been well documented, there have been no studies exploring angiogenesis in a VCEM microenvironment.

Given that the *in vivo* extracellular environment provides optimal biochemical and biophysical cues to guide cellular behaviours, the current study aimed to provide a potential strategy for vascular regeneration using engineering vessel grafts that have cell-derived biomimetic VCEM microenvironment. A decellularized VCEM could provide a cell-type specific microenvironment to direct cell redistribution via selective vascular cell adhesion. Specifically, substantially increased HUVEC adhesion behaviour was achieved upon culture with EHUVEC. In contrast, this beneficial effect was impaired by EHSMC. In fact, the adhesion of HUVECs was significantly lower upon culture with EHSMC than TCP. Similarly, compared with TCP, EHSMC promoted HVSMC adhesion, while EHUVEC reduced HVSMC adhesion even lower than TCP. These results demonstrate that the VCEM has cell type-specific characteristics. Thus, specific VCEM can be designed to control vascular cell behaviours, notably promoting the adhesion of cells from which they originate and inhibiting other vascular cells. By extension, it could be hypothesized that the microenvironment was better re-cellularized by the cells from which it came at the time of culture for 3D culture conditions. Indeed, the 3D EHUVEC in bEVG retains the effect analogous to the one that we discovered in the EHUVEC. Moreover, 3D EHSMC signalled HVSMCs to repopulate in the grafts. The implanted engineered vessel grafts became progressively more re-cellularized by the host cells, and our finding that the hierarchical organization was significantly optimized over time supports this

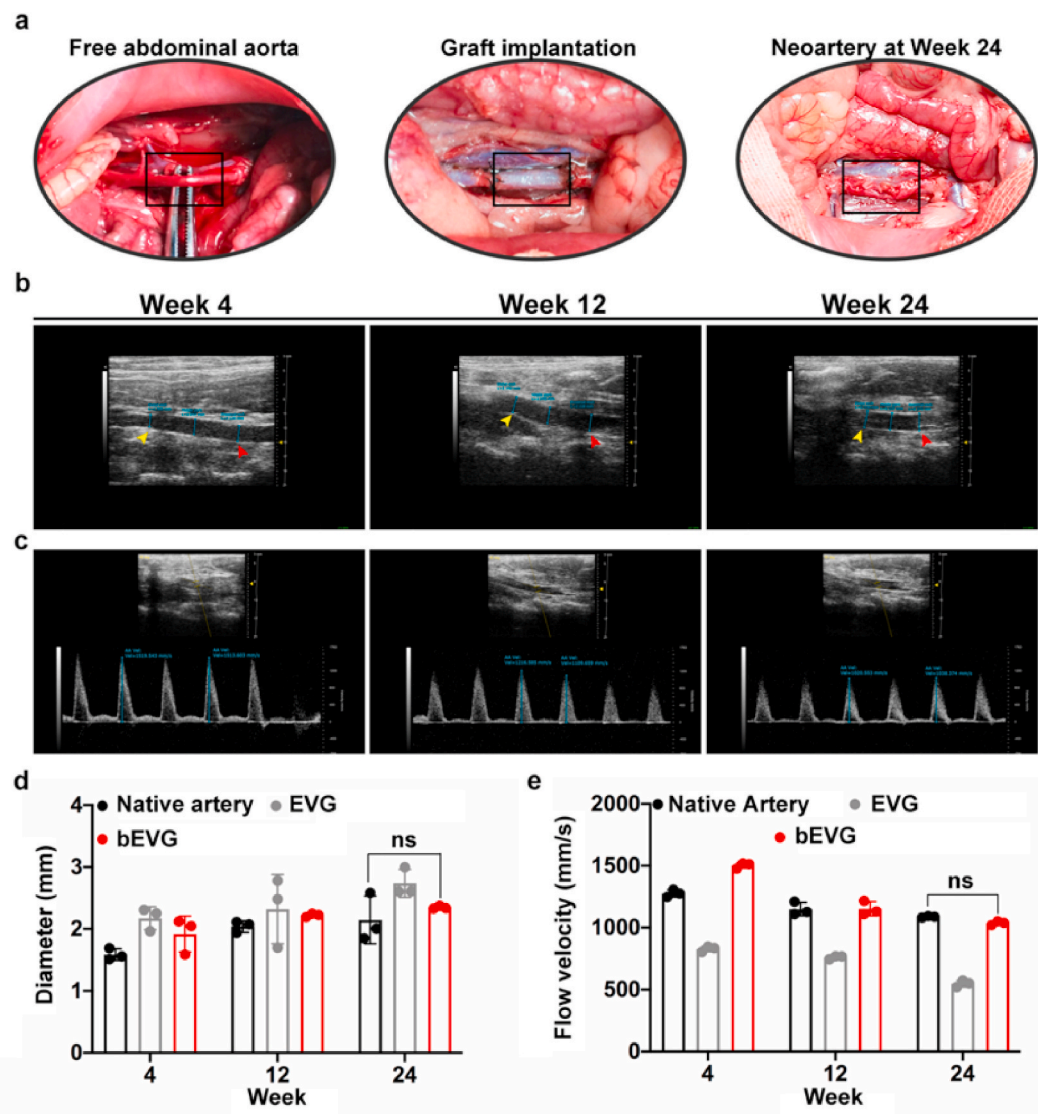


Fig. 6. Transplantation and ultrasonic analysis of bEVGs. (a) Images of bEVGs after implantation in rats. The black boxes indicate the replacement sites. (b) Ultrasound B-mode images of bEVGs. Yellow arrow: telecentric end of the bEVG; red arrow: proximal end of the bEVG. (c) Postoperative Doppler ultrasound measurements of bEVG blood flow velocity. (d) Quantification of the mid-neoartery diameter during the study. (e) Quantification of blood flow velocity in neoartery. (For interpretation of the references to color in this figure legend, the reader is referred to the Web version of this article.)

hypothesis.

Differential adhesion of vascular cells mediated by Eya3 is the basis of VCEM cell specificity. Because Eya is associated with 'ectopic' eyes, the Eya-mediated signalling response to 3D VCEM microenvironment may contribute to cellular localization [35,49]. The results showed that the VCEM conditions facilitated Eya3 expression in the vascular cells from which they originated, and Eya3 expression was inhibited in other vascular cells, leading to the committed localization of cell type-specific vascular cells. The Notch1-delta-like 4 (Dll4) signalling pathway plays critical roles in controlling multiple aspects of vascular development, ranging from proliferation, motility, and lumen formation to vessel stability and cell fate determination [50–52]. For certain types of vascular cells, the key factors of the Notch signalling pathway, including Notch1 and Dll4, were up-regulated by their derived ECMs; these key factors were down-regulated by ECMs from other vascular cells, indicating that the VCEM can affect Notch signalling pathway activation. Experiments using the Notch1 inhibitor DAPT revealed that DAPT significantly inhibited Notch1 expression, and Eya3 expression decreased accordingly. Interestingly, results for DAPT-treated vascular cells cultured in their derived ECM were similar to those cultured in

ECMs from other vascular cells. These findings reveal key roles for Notch signalling in luminal cell commitment. The effects of VCEM in regulating selective cell adhesion correlated with Eya3 expression levels, and the process depended on the activation of Notch signalling.

Structural and hierarchical anisotropy underlies the structure-function relationship of most living tissues [43,53]. Living cells reside within an intricate milieu of soluble biomolecules, cell-cell interactions, and cellular microenvironment. For blood vascular tissues, the structural anisotropy and hierarchical organization of the VCEM determine their specialized functions [54]. This study provides a proof of principle for committed cell localization using reconstituted VCEM microenvironment and suggests that VCEM systems could be used to regulate vascular angiogenesis by guiding the redistribution and localization of vascular cells. In addition, this study developed 3D VCEM *in vitro* that provided ECM cues while retaining the appropriate microtopographical features and microarchitectural structures for blood vascular tissue regeneration. PCL makes a good scaffold for self ready vascular graft applications due to its excellent mechanical properties, slow degradation rate, and good biocompatibility [9], however, in the long run, its vascular wall regeneration is insufficient, which is the driving force for

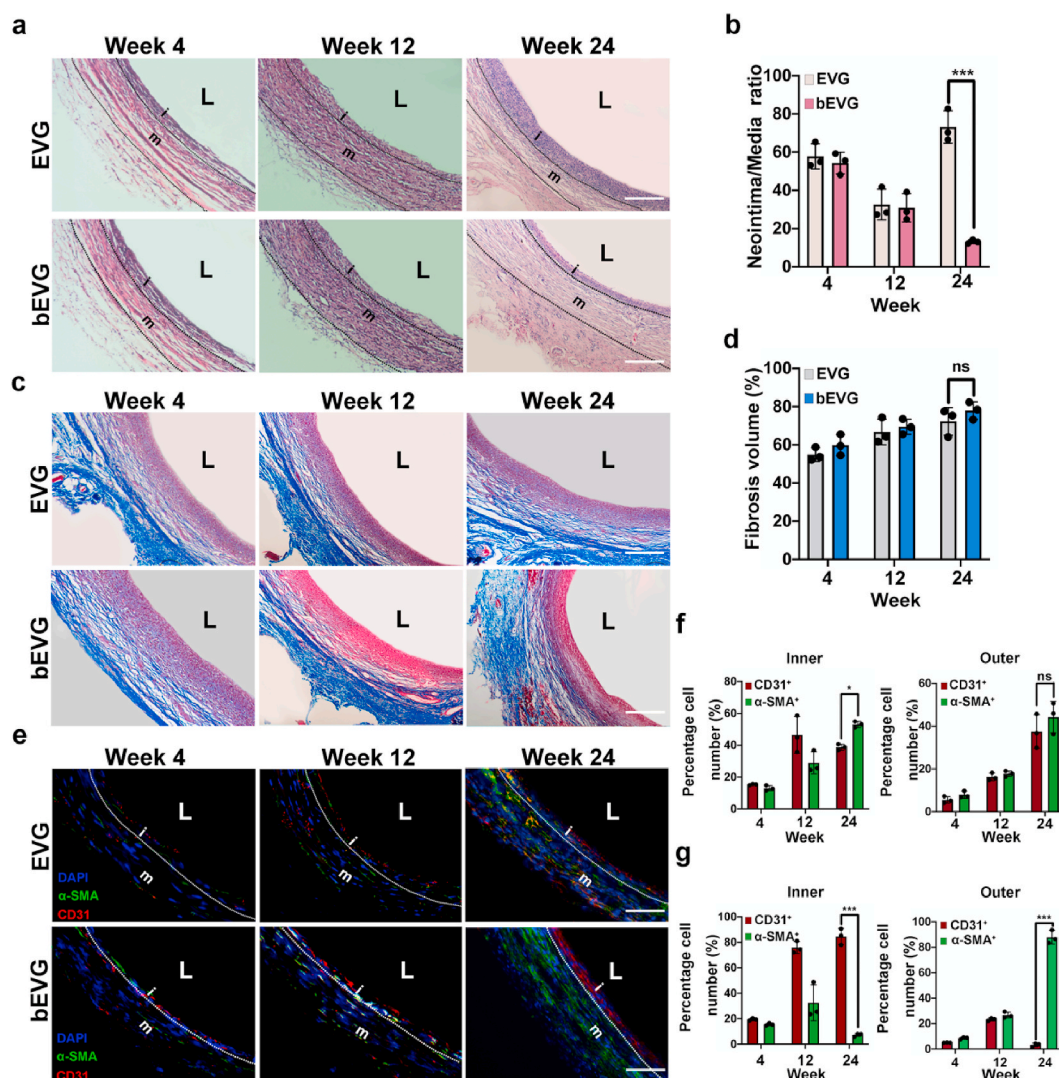


Fig. 7. Representative routine staining images of EVGs and bEVGs after implantation. (a) HE images showing pink-stained ECM and increased cell infiltration with time. i: neointima; m: medial layer; the borders are delineated by the black dashed lines. (b) Quantification of the neointima-to-media ratio. (c) MT images of blue-stained collagen fibres. Samples were explanted 4, 12, and 24 weeks after implantation, and sections were taken from the mid-graft regions. (d) Quantification of the fibrosis volumes of the neoarteries. (e) Immunofluorescence staining of explanted vascular grafts sections for CD31 (red) and α -SMA (green). The boundaries between the neointima and medial layers are delineated by the white dashed lines. The nuclei (blue) were counterstained with DAPI. (f) Quantification of the percentages of α -SMA⁺ or CD31⁺ in the inner and outer layers of explanted EVG. (g) Quantification of the percentages of α -SMA⁺ or CD31⁺ in the inner and outer layers of explanted bEVG. L: neoartery lumen. Scale bars = 100 μ m. (For interpretation of the references to color in this figure legend, the reader is referred to the Web version of this article.)

the work presented here. Therefore, ECM cues were integrated into the universal material to fabricate the 3D EHUVCE scaffold. 3D printing further enables construction of mimicking the defining features of native vascular intimal. As for 3D EHSMC, BC comfortably benefits from its unique properties such as a high permeability, high water-holding capacity, good biocompatibility, low toxicity and comparable to values of interest like the vasculature strength [55]. The prepared biomimetic 3D VCEM was capable of recapitulating a vascular cell type-specific 3D microenvironment to facilitate the appropriate niche location of cells by regulating their selective adhesion. Finally, the vascular cells cultured *in vitro* were surrounded by a biomimetic 3D microenvironment with vascular cell type-specific biochemical and biophysical cues similar to those *in vivo*. The study provides insight into optimizing the design and development of biomaterials to improve the remodelling of the vascular microenvironment.

Cell type-specific ECMs can provide a multifunctional system for regenerative medicine. However, due to the difficulty of structural reconstruction, the relevant research is often limited to the ECM itself,

and the 3D structure cannot be reproduced *in vitro*. In this study, bio-engineered vascular grafts containing 3D EHUVCE and EHSMC were constructed to regulate vascular cell localization. The cell type-specific VCEM was combined with the surface topographies of the grafts to create the synergistic effects of biochemical and biophysical cues. When using transplantation into an abdominal aorta vascular replacement rat model, good therapeutic efficacy and significant improvements in vascular remodelling and regeneration dependent on proper cell adhesion were found. Cells were capable of transitioning into myogenic or endothelial cell types based on colocalization with α -SMA or CD31, respectively. CD31⁺ cells appeared first throughout the graft; in subsequent explants, CD31⁺ cells were primarily in the inner layer, and α -SMA⁺ cells were recruited to the outer layer. Although cell type-specific VCEM show exciting therapeutic effects as cell culture systems for regulating the selective behaviour of cells, additional studies with more time points will be needed to determine whether these cells change their phenotype to become other cells in the future. These studies could lead to a better understanding of the autonomic homing action of cells

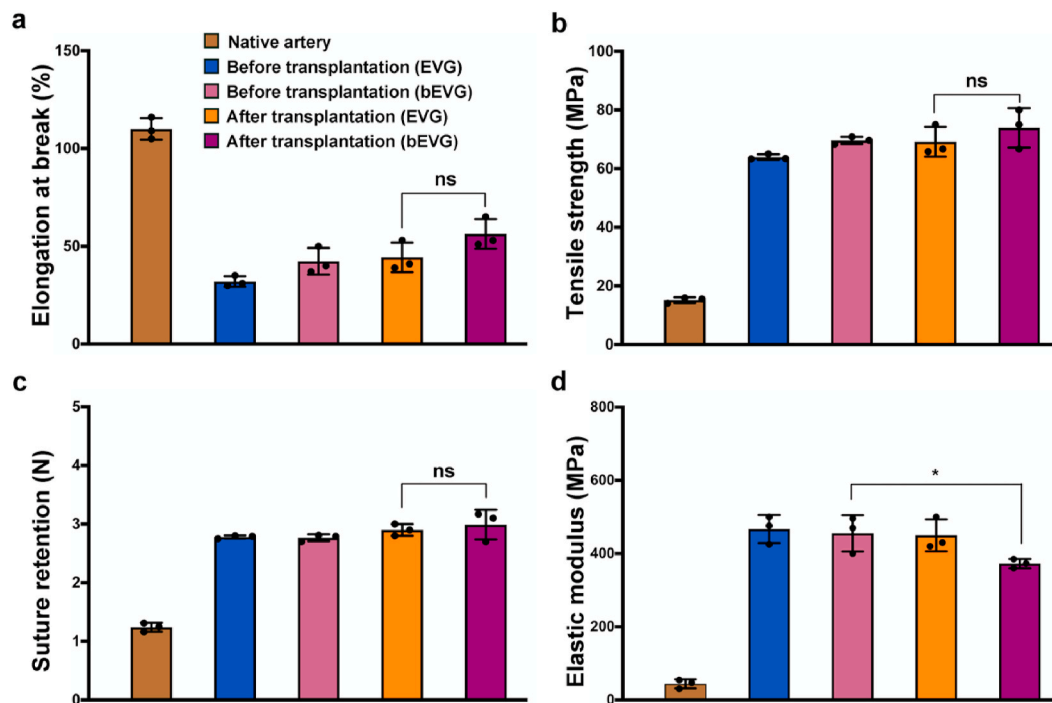


Fig. 8. Tensile properties of the vascular grafts. (a) Elongation at break. (b) Ultimate tensile strength. (c) Suture retention. (d) Young's modulus. The longitudinal tensile properties of the vascular grafts were compared before transplantation, 24 weeks after transplantation, and to native arteries. * $P < 0.05$.

that could be applied for guiding the remodelling and regeneration of heterogeneous tissues. Detailed information about the VCEM composition and whether it differs between the two cell types is currently underway supports cell type-specific ECM a new regulatory component to the self-organization of multicellular systems.

5. Conclusion

This study reveals a potential strategy for vascular regeneration using engineered vessel grafts with cell-derived biomimetic microenvironment. The findings represent a proof of principle for vascular cell localization in distinct cellular microenvironment and provide a novel perspective for further investigations on the controlled regeneration of heterogeneous tissues. The 3D microenvironment with VCEM acts as potent regulators that influence the native match between cell type and spatial patterning by providing enriched biochemical and biophysical cues. Moreover, the distinct cellular microenvironment has the potential to generate vascular tissue with high functionality and therapeutic efficacy, and the *in vivo*-mimicking model system established in this study may be useful for understanding the inherent factors involved in the regulation of cell fate and function for vascular tissue regeneration.

CRediT authorship contribution statement

Jian Wang: Formal analysis, Data curation. **Xun Yang:** Investigation. **Miaomiao Xu:** Data curation. **Hui Liu:** Software. **Lijun Liu:** Resources. **Zhikai Tan:** Writing – review & editing, Writing – original draft, Funding acquisition, Formal analysis, Conceptualization.

Declaration of competing interest

The authors declare that they have no known competing financial interests or personal relationships that could have appeared to influence the work reported in this paper.

Data availability

Data will be made available on request.

Acknowledgements

This study was financially supported by the Research and Development Plan of Key Fields in Hunan Province (No. 2022SK2027), Natural Science Foundation of Guangdong Province (No. 2023A1515011463), High-end Foreign Experts Recruitment Plan of China (No. G2023160019L), Shanghai Key Laboratory of Peripheral Nerve and Microsurgery (20DZ2270200), NHC Key Laboratory of Hand Reconstruction (Fudan University), Institute of Hand Surgery, Shanghai.

Appendix A. Supplementary data

Supplementary data to this article can be found online at <https://doi.org/10.1016/j.mtbio.2024.101033>.

References

- [1] L.E. Niklason, J.H. Lawson, Bioengineered human blood vessels, *Science*. 370 (6513) (2020) eaaw8682.
- [2] J.S. Luo, L.F. Qin, L.P. Zhao, L.Q. Gui, M.W. Ellis, Y. Huang, M.H. Kural, J.A. Clark, S. Ono, J. Wang, Y.F. Yuan, S.M. Zhang, X.Q. Cong, G.X. Li, M. Riaz, C. Lopez, A. Hotta, S. Campbell, G. Tellides, A. Dardik, L.E. Niklason, Y.B. Qyang, Tissue-engineered vascular grafts with advanced mechanical strength from human iPSCs, *Cell Stem Cell* 26 (2) (2020) 251–261.
- [3] J.H. Lawson, M.H. Glickman, M. Ilzecki, T. Jakimowicz, A. Jaroszynski, E.K. Peden, A.J. Pilgrim, H.L. Prichard, M. Guziewicz, S. Przywara, J. Szmidi, J. Turek, W. Witkiewicz, N. Zapotoczny, T. Zubilewicz, L.E. Niklason, Bioengineered human acellular vessels for dialysis access in patients with end-stage renal disease: two phase 2 single-arm trials, *Lancet* 387 (10032) (2016) 2026–2034.
- [4] R.D. Kirkton, M. Santiago-Maysonet, J.H. Lawson, W.E. Tente, S.L.M. Dahl, L. E. Niklason, H.L. Prichard, Bioengineered human acellular vessels recellularize and evolve into living blood vessels after human implantation, *Sci. Transl. Med.* 11 (485) (2019) eaau6934.
- [5] H. Yamanaka, T. Yamaoka, A. Mahara, N. Morimoto, S. Suzuki, Tissue-engineered submillimeter-diameter vascular grafts for free flap survival in rat model, *Biomaterials* 179 (2018) 156–163.
- [6] S.L.M. Dahl, A.P. Kypson, J.H. Lawson, J.L. Blum, J.T. Strader, Y.L. Li, R.J. Manson, W.E. Tente, L. DiBernardo, M.T. Hensley, R. Carter, T.P. Williams, H.L. Prichard,

- M.S. Dey, K.G. Begelman, L.E. Niklason, Readily available tissue-engineered vascular grafts, *Sci. Transl. Med.* 3 (68) (2011) 68ra9.
- [7] T. Mirabella, J.W. MacArthur, D. Cheng, C.K. Ozaki, Y.J. Woo, M.T. Yang, C. S. Chen, 3D-printed vascular networks direct therapeutic angiogenesis in ischaemia, *Nat. Biomed. Eng.* 1 (6) (2017) 83.
- [8] J.D. Drews, V.K. Pepper, C.A. Best, J.M. Szafron, J.P. Cheatham, A.R. Yates, K. N. Hor, J.C. Zbinden, Y.C. Chang, G.J.M. Mirhaidari, A.B. Ramachandra, S. Miyamoto, K.M. Blum, E.A. Onwuka, J. Zakkó, J. Kelly, S.L. Cheatham, N. King, J.W. Reinhardt, T. Sugiura, H. Miyachi, Y. Matsuzaki, J. Breuer, E.D. Heuer, T. A. West, T. Shoji, D. Berman, B.A. Boe, J. Asnes, M. Galantowicz, G. Matsumura, N. Hibino, A.L. Marsden, J.S. Pober, J.D. Humphrey, T. Shinoka, C.K. Breuer, Spontaneous reversal of stenosis in tissue-engineered vascular grafts, *Sci. Transl. Med.* 12 (537) (2020) eaax6919.
- [9] S. de Valence, J.C. Tille, D. Mugnai, W. Mrowczynski, R. Gurny, M. Moller, B. H. Walpoth, Long term performance of polycaprolactone vascular grafts in a rat abdominal aorta replacement model, *Biomaterials* 33 (2012) 38–47.
- [10] S. Verma, P.E. Smitko, R.D. Weisel, D. Bonneau, D. Latter, L. Errett, Y. LeClerc, S. E. Fremes, Should radial arteries be used routinely for coronary artery bypass grafting? *Circulation* 110 (5) (2004) E40–E46.
- [11] E. Bassat, Y.E. Mutlak, A. Genzelinakh, I.Y. Shadrin, K. Baruch Umansky, O. Yifa, D. Kain, D. Rajchman, J. Leach, D. Riabov Bassat, Y. Udi, R. Sarig, I. Sagi, J. F. Martin, N. Bursac, S. Cohen, E. Tzahor, The extracellular matrix protein agrin promotes heart regeneration in mice, *Nature* 547 (7662) (2017) 179–184.
- [12] A.N. Cho, Y. Jin, Y. An, J. Kim, Y.S. Choi, J.S. Lee, J. Kim, W.Y. Choi, D.J. Koo, W. Yu, G.E. Chang, D.Y. Kim, S.H. Jo, J. Kim, S.Y. Kim, Y.G. Kim, J.Y. Kim, N. Choi, E. Cheong, Y.J. Kim, H.S. Je, H.C. Kang, S.W. Cho, Microfluidic device with brain extracellular matrix promotes structural and functional maturation of human brain organoids, *Nat. Commun.* 12 (1) (2021) 4730.
- [13] E. Rossi, J. Guerrero, P. Aprile, A. Tocchio, E.A. Kappos, I. Gerges, C. Lenardi, I. Martin, A. Scherberich, Decoration of RGD-mimetic porous scaffolds with engineered and devitalized extracellular matrix for adipose tissue regeneration, *Acta Biomater.* 73 (2018) 154–166.
- [14] M.F. Zhu, W. Li, X.H. Dong, X.Y. Yuan, A.C. Midgley, H. Chang, Y.H. Wang, H. Y. Wang, K. Wang, P.X. Ma, H.J. Wang, D.L. Kong, In vivo engineered extracellular matrix scaffolds with instructive niches for oriented tissue regeneration, *Nat. Commun.* 10 (1) (2019) 4620.
- [15] G.G. Giobbe, C. Crowley, C. Luni, S. Campinoti, M. Khedr, K. Kretschmar, M.M. De Santis, E. Zambaiti, F. Michielin, L. Meran, Q. Hu, G. van Son, L. Urbani, A. Manfredi, M. Giomo, S. Eaton, D. Cacchiarelli, V.S.W. Li, H. Clevers, P. Bonfanti, N. Elvassore, P. De Coppi, Extracellular matrix hydrogel derived from decellularized tissues enables endodermal organoid culture, *Nat. Commun.* 10 (1) (2019) 5658.
- [16] Y. Jin, J.S. Lee, J. Kim, S. Min, S. Wi, J.H. Yu, G.E. Chang, A.N. Cho, Y. Choi, D. H. Ahns, S.R. Cho, E. Cheong, Y.G. Kim, H.P. Kim, Y. Kim, D.S. Kim, H.W. Kim, Z. Qian, H.C. Kang, S.W. Cho, Three-dimensional brain-like microenvironments facilitate the direct reprogramming of fibroblasts into therapeutic neurons, *Nat. Biomed. Eng.* 2 (7) (2018) 522–539.
- [17] J.K. Mouw, G.Q. Ou, V.M. Weaver, Extracellular matrix assembly: a multiscale deconstruction, *Nat. Rev. Mol. Cell Biol.* 15 (12) (2014) 771–785.
- [18] B. Yao, R. Wang, Y.H. Wang, Y.J. Zhang, T. Hu, W. Song, Z. Li, S. Huang, X.B. Fu, Biochemical and structural cues of 3D-printed matrix synergistically direct MSC differentiation for functional sweat gland regeneration, *Sci. Adv.* 6 (10) (2020) eaaz1094.
- [19] J.P. Guyette, J.M. Charest, R.W. Mills, B.J. Jank, P.T. Moser, S.E. Gilpin, J. R. Gershlak, T. Okamoto, G. Gonzalez, D.J. Milan, G.R. Gaudette, H.C. Ott, Bioengineering human myocardium on native extracellular matrix, *Circ. Res.* 118 (1) (2016) 56–72.
- [20] C. Park, K.S. Park, M.J. Jeong, H.B. Kim, I. Bae, K.S. Lim, M.X. Li, Y.J. Hong, D. K. Han, Y.K. Joong, A robustly supported extracellular matrix improves the intravascular delivery efficacy of endothelial progenitor cells, *Adv. Funct. Mater.* 31 (2021) 2100324.
- [21] T.T. Han, S. Toutounji, B.G. Amsden, L.E. Flynn, Adipose-derived stromal cells mediate *in vivo* adipogenesis, angiogenesis and inflammation in decellularized adipose tissue bioscaffolds, *Biomaterials* 72 (2015) 125–137.
- [22] C.J. Li, G.H. Zhen, Y. Chai, L. Xie, J.L. Crane, E. Farber, C.R. Farber, X.H. Luo, P. S. Gao, X. Cao, M. Wan, RhoA determines lineage fate of mesenchymal stem cells by modulating CTGF-VEGF complex in extracellular matrix, *Nat. Commun.* 7 (1) (2016) 11455.
- [23] J.F. Liu, H.Y. Long, D. Zeuschner, A.F.B. Rader, W.J. Polachek, H. Kessler, L. Sorokin, B. Trappmann, Synthetic extracellular matrices with tailored adhesiveness and degradability support lumen formation during angiogenic sprouting, *Nat. Commun.* 12 (1) (2021) 3402.
- [24] N. Facchinello, M. Astone, M. Audano, R.E. Oberkersch, M. Spizzotin, E. Calura, M. Marques, M. Crisan, N. Mitro, M.M. Santoro, Oxidative pentose phosphate pathway controls vascular mural cell coverage by regulating extracellular matrix composition, *Nat. Metab.* 4 (1) (2022) 123–140.
- [25] P. Du, M. Suhaeri, S.S. Ha, S.J. Oh, S.H. Kim, K. Park, Human lung fibroblast-derived matrix facilitates vascular morphogenesis in 3D environment and enhances skin wound healing, *Acta Biomater.* 54 (2017) 333–344.
- [26] C. Mandrycky, B. Hadland, Y. Zheng, 3D curvature-instructed endothelial flow response and tissue vascularization, *Sci. Adv.* 6 (38) (2020) eabb3629.
- [27] C. O'Connor, E. Brady, Y. Zheng, E. Moore, K.R. Stevens, Engineering the multiscale complexity of vascular networks, *Nat. Rev. Mater.* 7 (9) (2022) 702–716.
- [28] D.T. Li, W.Z. Xue, M. Li, M. Dong, J.W. Wang, X.D. Wang, X.Y. Li, K. Chen, W. J. Zhang, S. Wu, Y.Q. Zhang, L. Gao, Y.J. Chen, J.F. Chen, B.O. Zhou, Y. Zhou, X. B. Yao, L. Li, D.Q. Wu, W.J. Pan, VCAM-1(+) macrophages guide the homing of HSPCs to a vascular niche, *Nature* 564 (7734) (2018) 119–124.
- [29] A.A. Khalili, M.R. Ahmad, A review of cell adhesion studies for biomedical and biological applications, *Int. J. Mol. Sci.* 16 (2015) 18149–18184.
- [30] J.A. Brassard, M. Nikolaev, T. Hubscher, M. Hofer, M.P. Lutolf, Recapitulating macro-scale tissue self-organization through organoid bioprinting, *Nat. Mater.* 20 (1) (2021) 22–29.
- [31] K. Bentley, C.A. Franco, A. Philippides, R. Blanco, M. Dierkes, V. Gebala, F. Stanchi, M. Jones, I.M. Aspalter, G. Cagna, S. Westrom, L. Claesson-Welsh, D. Vestweber, H. Gerhardt, The role of differential VE-cadherin dynamics in cell rearrangement during angiogenesis, *Nat. Cell Biol.* 16 (4) (2014) 309–321.
- [32] G. Serini, D. Valdembrì, S. Zanivan, G. Morterra, C. Burkhardt, F. Caccavari, L. Zammataro, L. Primo, L. Tamagnone, M. Logan, M. Tessier-Lavigne, M. Taniguchi, A.W. Puschel, F. Bussolino, Class 3 semaphorins control vascular morphogenesis by inhibiting integrin function, *Nature* 424 (6947) (2003) 391–397.
- [33] G. Mana, F. Clapero, E. Panieri, V. Panero, R.T. Bottcher, H.Y. Tseng, F. Saltarin, E. Astanina, K.I. Wolanska, M.R. Morgan, M.J. Humphries, M.M. Santoro, G. Serini, D. Valdembrì, PPIA1 drives active $\alpha 5 \beta 1$ integrin recycling and controls fibronectin fibrillogenesis and vascular morphogenesis, *Nat. Commun.* 7 (1) (2016) 13546.
- [34] Z.Q. Wu, R.G. Rowe, K.C. Lim, Y.S. Lin, A. Willis, Y. Tang, X.Y. Li, J.E. Nor, I. Maillard, S.J. Weiss, A Snail1/Notch1 signalling axis controls embryonic vascular development, *Nat. Commun.* 5 (1) (2014) 3998.
- [35] W. Dai, A. Peterson, T. Kenney, H. Burrous, D.J. Montell, Quantitative microscopy of the *Drosophila* ovary shows multiple niche signals specify progenitor cell fate, *Nat. Commun.* 8 (1) (2017) 1244.
- [36] V.C. Luca, K.M. Jude, N.W. Pierce, M.V. Nachury, S. Fischer, K.C. Garcia, Structural basis for Notch1 engagement of delta-like 4, *Science* 347 (6224) (2015) 847–853.
- [37] R.Y. Huang, J. Wang, H.X. Chen, X.L. Shi, X.C. Wang, Y.H. Zhu, Z.K. Tan, The topography of fibrous scaffolds modulates the paracrine function of Ad-MSCs in the regeneration of skin tissues, *Biomater. Sci.* 7 (10) (2019) 4248–4259.
- [38] H. Chen, Y. Cheng, X. Wang, J. Wang, X. Shi, X. Li, W. Tan, Z. Tan, 3D printed *in vitro* tumor tissue model of colorectal cancer, *Theranostics* 10 (26) (2020) 12127–12143.
- [39] C. Bakolitsa, D.M. Cohen, L.A. Bankston, A.A. Bobkov, G.W. Cadwell, L. Jennings, D.R. Critchley, S.W. Craig, R.C. Liddington, Structural basis for vinculin activation at sites of cell adhesion, *Nature* 430 (6999) (2004) 583–586.
- [40] I. Rebay, Multiple functions of the Eya phosphotyrosine phosphatase, *Mol. Cell Biol.* 36 (5) (2016) 668–677.
- [41] V. Weichselberger, P. Dondl, A.K. Classen, Eya-controlled affinity between cell lineages drives tissue self-organization during *Drosophila* oogenesis, *Nat. Commun.* 13 (1) (2022) 6377.
- [42] J.X. Zhou, J.B. Han, S.M. Chen, Y. Xu, Y.G. Kong, B.K. Xiao, Z.Z. Tao, gamma-secretase inhibition combined with cisplatin enhances apoptosis of nasopharyngeal carcinoma cells, *Exp. Ther. Med.* 3 (2) (2012) 357–361.
- [43] Z. Wang, W.J. Lee, B.T.H. Koh, M. Hong, W. Wang, P.N. Lim, J. Feng, L.S. Park, M. Kim, E.S. Thian, Functional regeneration of tendons using scaffolds with physical anisotropy engineered via microarchitectural manipulation, *Sci. Adv.* 4 (10) (2018) eaat4537.
- [44] P.L. Wu, L.N. Wang, W. Li, Y. Zhang, Y.F. Wu, D.K. Zhi, H.J. Wang, L.Y. Wang, D. L. Kong, M.F. Zhu, Construction of vascular graft with circumferentially oriented microchannels for improving artery regeneration, *Biomaterials* 242 (2020) 119922.
- [45] X.Y. Yuan, W. Li, B. Yao, Z. Li, D.L. Kong, S. Huang, M.F. Zhu, Tri-layered vascular grafts guide vascular cells' native-like arrangement, *Polymers* 14 (7) (2022) 1370.
- [46] N. Facchinello, M. Astone, M. Audano, R.E. Oberkersch, M. Spizzotin, E. Calura, M. Marques, M. Crisan, N. Mitro, M.M. Santoro, Oxidative pentose phosphate pathway controls vascular mural cell coverage by regulating extracellular matrix composition, *Nat. Metab.* 4 (1) (2022) 123–140.
- [47] C. Bonnans, J. Chou, Z. Werb, Remodelling the extracellular matrix in development and disease, *Nat. Rev. Mol. Cell Biol.* 15 (12) (2014) 786–801.
- [48] F.M. Watt, W.T.S. Huck, Role of the extracellular matrix in regulating stem cell fate, *Nat. Rev. Mol. Cell Biol.* 14 (8) (2013) 467–473.
- [49] X. Li, K.A. Oghi, J. Zhang, A. Krone, K.T. Bush, C.K. Glass, S.K. Nigam, A. K. Aggarwal, R. Maas, D.W. Rose, M.G. Rosenfeld, Eya protein phosphatase activity regulates Six1-Dach-Eya transcriptional effects in mammalian organogenesis, *Nature* 426 (6964) (2003) 247–254.
- [50] R. Lim, T. Sugino, H. Nolte, J. Andrade, B. Zimmermann, C. Shi, A. Doddaballapur, Y.T. Ong, K. Wilhelm, J.W.D. Fasse, A. Ernst, M. Kaulich, K. Husnjak, T. Boettger, S. Guenther, T. Braun, M. Kruger, R. Benedito, I. Dikic, M. Potente, Deubiquitinase USP10 regulates Notch signaling in the endothelium, *Science* 364 (6436) (2019) 188–193.
- [51] W. Luo, I. Garcia-Gonzalez, M. Fernandez-Chacon, V. Casquero-Garcia, M. S. Sanchez-Munoz, S. Muhleder, L. Garcia-Ortega, J. Andrade, M. Potente, R. Benedito, Arterialization requires the timely suppression of cell growth, *Nature* 589 (7842) (2021) 437–441.
- [52] M.E. Pitulescu, I. Schmidt, B.D. Giaimo, T. Antoine, F. Berkenfeld, F. Ferrante, H. Park, M. Ehling, D. Biljes, S.F. Rocha, U.H. Langen, M. Stehling, T. Nagasawa, N. Ferrara, T. Borggreve, R.H. Adams, Dll4 and Notch signalling couples sprouting angiogenesis and artery formation, *Nat. Cell Biol.* 19 (8) (2017) 915–927.

- [53] P. Kanchanawong, D.A. Calderwood, Organization, dynamics and mechanoregulation of integrin-mediated cell-ECM adhesions, *Nat. Rev. Mol. Cell Biol.* 24 (2) (2023) 142–161.
- [54] C. Bonnans, J. Chou, Z. Werb, Remodelling the extracellular matrix in development and disease, *Nat. Rev. Mol. Cell Biol.* 15 (12) (2014) 786–801.
- [55] Y. Li, K. Jiang, J. Feng, J. Liu, R. Huang, Z. Chen, J. Yang, Z. Dai, Y. Chen, N. Wang, W. Zhang, W. Zheng, G. Yang, X. Jiang, Construction of small-diameter vascular graft by shape-memory and self-rolling bacterial cellulose membrane, *Adv. Healthcare Mater.* 6 (11) (2017) 1601343.